Pergamon

Int. J. Solids Structures Vol. 35, Nos. 5–6, pp. 457–477, 1998

0020–7683/98 $19.00 + .00

PII: S0020–7683(97)00032–2

AN ANALYTICAL MODEL FOR THERMAL RESIDUAL INTERFACE-STRESSES IN CONTINUOUS-FIBER-REINFORCED COMPOSITES

CHAO ZHANG
Department of Aircraft Structures, Shanghai Aircraft Research Institute, P.O. Box 232–003, Shanghai 200232, P.R. China

and

HSIEN-YANG YEH†
Mechanical Engineering Department, California State University at Long Beach, Long Beach, CA 90840, U.S.A.

(*Received* 27 *December* 1995; *in revised form* 6 *January* 1997)

Abstract—An analytical model is proposed to predict thermal stresses at the fiber-matrix interface in continuous-fiber-reinforced composites. First, the initial imperfections in fiber layout are introduced, which are assumed to be the extensional fiber misalignment and the local fiber misalignment respectively. Then, the displacement fields subjected to thermal loadings are found for the two cases. The former is based on Timoshenko beam theory and classical elasticity and the latter based on variational principles. Finally, the thermal residual stresses are determined using the linear stress-strain relationships. Numerical results show that temperature drop will result in residual shear stress at the fiber-matrix interface that can cause debonding and micro-cracks in matrix. This study is extremely useful to understand the microscopic failure mechanism for fiber-reinforced composites.

NOMENCLATURE

A, B	constants in fiber displacements due to fiber micro-bending
B_i	amplitude of initial fiber curvature
$C_i, c, c_i, \bar{c}_i$	constants
$D_i, d_i, \bar{d}_i$	constants
e	ratio of amplitude to half wavelength of initial fiber curvature
H_i, h, J_i, K	parameters
I_f	moment of initial of each fiber
L	wavelength of initial fiber curvature
M	bending moment
m_i	parameter
$P_i, \bar{P}_i, p$	constants
p'	variation of axial loading in each fiber due to fiber micro-bending
Q	shear loading
$Q_i, \bar{Q}_i, q$	constants
r_f, r_m	fiber radius and surrounding matrix radius in the coaxial cylinder model
T	temperature change
U_f, V_f	axial displacement and deflection of each fiber due to fiber micro-bending
V_i	deflection of initial fiber curvature
U_m, V_m	axial and lateral displacements of the matrix due to fiber micro-bending
v_f	fiber volume fraction
W	work
$u^{(f)}, w^{(f)}$	radial and axial displacements of each fiber from the coaxial cylinder model
$u^{(m)}, w^{(m)}$	radial and axial displacements of the matrix from the coaxial cylinder model
r, θ, x	cylindrical coordinates
$\bar{x}, \bar{y}$	two-dimensional Cartesian coordinates for the matrix
x, y	two-dimensional Cartesian coordinates for each fiber
α	parameter
λ	nondimensional wavelength of initial fiber curvature
$\sigma_r^{(f)}, \sigma_\theta^{(f)}, \sigma_x^{(f)}$	thermal stresses in fibers from the coaxial cylinder model
$\sigma_r^{(m)}, \sigma_\theta^{(m)}, \sigma_x^{(m)}$	thermal stresses in the matrix from the coaxial cylinder model
$\varepsilon_r^{(f)}, \varepsilon_\theta^{(f)}, \varepsilon_x^{(f)}$	strains in the fibers from the coaxial cylinder model

† Author to whom correspondence should be addressed.

$\varepsilon_r^{(m)}$, $\varepsilon_\theta^{(m)}$, $\varepsilon_x^{(m)}$	strains in the matrix from the coaxial cylinder model
σ_r, τ_r	interface stresses at the right side of a fiber in the developed model
σ_l, τ_l	interface stresses at the left side of a fiber in the developed model
σ_{xm}, $\sigma_{\theta m}$, τ_{xym}	additional thermal stresses in the matrix due to fiber micro-bending
$\sigma_{\max}$, $\tau_{\max}$	maximum interface stresses
$\Psi(y)$, $\Phi(y)$	displacement functions
Π	potential energy
Π_f, Π_{ff}, Π_m, Π_{mf}	energies
Δ^*, Δ^{**}	parameters.

1. INTRODUCTION

It is well known that thermal residual stresses arise from mismatch in thermal expansion coefficients between fibers and the surrounding matrix in fiber-reinforced composites when composites cool, down from the curing temperature to the room temperature. The distribution of thermal residual stresses is three-dimensional and very complicated, dependent on the volume fraction and material properties of fiber and matrix. Thermal residual stresses not only degrade composites' damage behavior and fracture toughness but also lower impact strength and fatigue life.

Generally, the thermal stress field is described using a coaxial cylinder model (Iesan, 1980; Mikata and Taya, 1985; Pagano and Tandon, 1988; Jayaraman and Reifsnider, 1993; Powell *et al.*, 1993). In this model, it is assumed that the fibers are in alignment in the matrix and the stresses and displacements are continuous at the fiber-matrix interface. The outer matrix surface is stress free (Fig. 1). The solution from the coaxial cylinder model demonstrates that there exists only thermal residual lateral stress at the interface but no shear stresses except for near the stress free surface (such as fiber-breakage), and an axial compressive loading arising in each fiber with temperature drop. Because interface debonding depends on the magnitudes of both tensile lateral stress and shear stresses at the interface (the effect of lateral stress on interface debonding is negligible if it is compressive) (Brewer and Lagace, 1988), the results from the coaxial cylinder model that lateral stress is compressive when temperature drops and no shear stress exists at the interface could not illustrate the debonding phenomena, which may exist in fiber-reinforced composites after curing and is the fundamental mode of matrix damage.

In fact, fibers in composite materials are not straight. In the wet lay-up manufacturing process, fibers will springback in the initial cycle of curing, in which the matrix changes from a liquid state to a gel state with increasing degree of crosslinking (Strong, 1989). In the prepreg manufacturing process, the escape of entrapped air, water, or volatile and the flow-out of excess resin from the parts in the curing cycle may move the fibers (Hajjati, 1994). The initial fiber curvature will lower the compressive strength of composite materials. More detailed descriptions of this mechanism are available in literature (Hahn and Sohi, 1986; Lanir and Fung, 1972). In order to reduce the magnitude of initial fiber curvature, some special manufacturing methods have been taken. For example, in the process of filament winding, adequate fiber tension is required to collimate the fibers on the mandrel. The fiber tension is created by pulling the fibers through a number of fiber guides placed

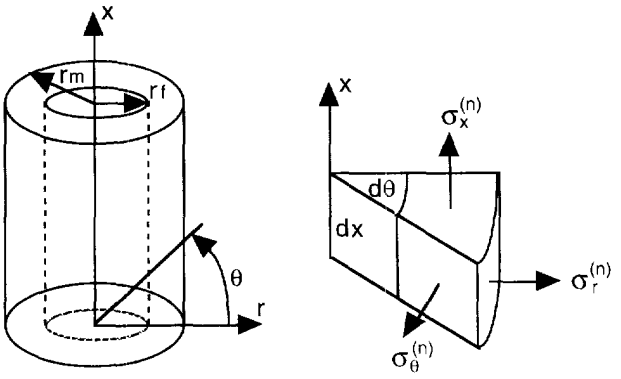

Fig. 1. The configuration of coaxial cylinder model and stress components.

between the creels and the resin bath (Strong, 1989). Maybe, Herrman *et al.* (1967) were the first authors who studied the existence of initial fibre curvature and its effect on the compressive response of composite materials. Then, investigations on this topic were conducted by Hanasaki and Hasegawa (1974), Davis (1975), Hahn and Williams (1984), Yeh and Teply (1988), etc. Generally, an ideal assumption of parallel sinusoidal waves with given wavelength and amplitude was accepted in these papers although in fact the initial fiber curvature is not parallel to each other, and even has a random characteristic (Slaughter and Fleck, 1994). Davis (1975) found that the initial fiber curvature has a wave-like shape and measured the initial fiber deflection of a boron/epoxy system with an amplitude to wavelength ratio in order of 10^{-2} by a micrographic method.

The theory of elastic stability (Timoshenko and Gere, 1961) has shown that an axial compressive loading bends a beam with initial curvature even though the loading is substantially lower than the buckling strength and the magnitude of the beam's deflection is not linearly dependent on the loading. Hence, it can be deduced that the axial compressive loading in the fiber due to temperature decrease will bend the fiber with initial imperfections, thus resulting in the existence of residual shear stresses at the fiber-matrix interface. Because the coaxial cylinder model neglects the initial fiber imperfections, it predicts no existence of residual shear stresses in the fiber-matrix system. Kalantar and Drzal (1990) and Banbaji (1988) have measured the interfacial shear strength by single fibre pull-out tests. They concluded that the interface shear stress equal to or greater than the strength could lead to debonding. The thermal residual interface shear stress is sufficiently high to suggest that the interface can be debonded at low temperature.

The main purpose of this paper is to study thermal residual stresses, especially shear stress component, at the fiber-matrix interface in composite materials from a standpoint of micromechanics. The available micromechanics analyses are approximate in this paper because of the assumptions of idealized shapes of initial fiber curvature, fiber packing symmetry and unmeasurable properties of anisotropic fibers, etc. The initial fiber curvature is approximated as two idealized modes, namely extensional fiber misalignments (Herrman *et al.* 1967; Hanasaki and Hasegawa, 1974; Davis, 1975), and local fiber misalignments (Yeh and Teply, 1988; Lessard and Chang, 1991). Both the nodes of initial fiber curvature may exist in fiber-reinforced composites. The extensional fiber misalignments may arise from uniform springback of fibers in the uncured matrix, while the local fiber misalignments may arise from local movement of fibers in the uncured matrix due to internal disturbances (such as flow of resin and escape of entrapped volatile, etc.).

This paper develops an analytical model to determine thermal residual stresses at the fiber-matrix interface in unidirectional composites. First, the axial compressive loadings in the fibers due to temperature decrease are determined by the coaxial cylinder model. Then, the compressive responses of fibers for two cases, corresponding to the shapes of initial fiber imperfections, are considered under the action of axial compressive loadings. One is the extensional fiber micro-bending model (abbreviation EFB). In this analysis, the displacements of fiber and matrix are solved by Temoshenko beam theory and classical elasticity respectively. The conditions of traction and displacement continuity at the fiber-matrix interface are satisfied exactly. The other is the local fiber micro-bending model (abbreviation LFB). In this analysis, the displacements of the fiber-matrix system are determined by the principle of minimizing potential energy and variational method. From the displacements, the thermal residual interface stresses are obtained using the linear stress-strain relationships. The influence of initial fiber curvature, fiber volume fraction and temperature decrease on thermal residual shear stress at the fiber-matrix interface are discussed with the numerical results of T300/5222 composites.

2. BASIC ASSUMPTIONS

The basic assumptions in the present analysis are:

1. The fibers with circular cross-sections are uniformly distributed in the matrix and infinitely long in the longitudinal direction.

2. Both fiber and matrix are linearly elastic.
3. The displacements are continuous at the fiber-matrix interface (i.e., no interfacial slip).
4. The temperature distribution is uniform and the constituent material properties do not vary with temperature.
5. The initial imperfections of each fiber due to manufacturing process are identical and do not result in the initial stresses in the fiber-matrix system before composite curing.
6. There are two steps for the present analysis: the axial compressive loading in each fiber due to temperature decrease is determined by the coaxial cylinder model, then the compressive response of the fibers with initial imperfections from the compressive axial loadings is determined by EFB model or LFB model. Hence, the total thermal residual stresses are summations of stresses in the fiber-matrix system from the coaxial cylinder model (i.e., before fiber micro-bending) and additional stresses only due to the response of fiber micro-bending.

3. THERMAL RESIDUAL STRESSES FROM COAXIAL CYLINDER MODEL

In order to develop the model presented in this paper, the thermal residual stresses in the fiber-matrix system in which no fiber micro-bending occurs must be obtained at first. Lame's method is employed here. Because the initial fiber deflection is a small magnitude compared with the wavelength of bending fiber (Davis, 1975), we can approximately neglect the effect of the fiber initial deflection (i.e., assume that the slope ratio of initial fiber curvature is equal to zero).

Consider a concentric model shown in Fig. 1. This model omits the constraint effect of the surrounding composite. r_f and r_m denote the radius of fiber and the radius of surrounding matrix. It is obvious that fiber volume fraction v_f is:

$$v_f = \frac{r_f^2}{r_m^2}. \tag{1}$$

Because the fiber is transversely isotropic and the matrix is isotropic, the strain-stress relations, taking into account thermal expansions and temperature change, for the fibers and the matrix are:

$$\varepsilon_x^{(f)} - \alpha_1^{(f)} T = \frac{\sigma_x^{(f)}}{E_1^{(f)}} - \frac{\mu_{12}^{(f)}}{E_1^{(f)}} \sigma_r^{(f)} - \frac{\mu_{12}^{(f)}}{E_1^{(f)}} \sigma_\theta^{(f)} \tag{2.a}$$

$$\varepsilon_r^{(f)} - \alpha_2^{(f)} T = \frac{\sigma_r^{(f)}}{E_2^{(f)}} - \frac{\mu_{23}^{(f)}}{E_2^{(f)}} \sigma_\theta^{(f)} - \frac{\mu_{12}^{(f)}}{E_1^{(f)}} \sigma_x^{(f)} \tag{2.b}$$

$$\varepsilon_\theta^{(f)} - \alpha_2^{(f)} T = \frac{\sigma_\theta^{(f)}}{E_2^{(f)}} - \frac{\mu_{23}^{(f)}}{E_2^{(f)}} \sigma_r^{(f)} - \frac{\mu_{12}^{(f)}}{E_1^{(f)}} \sigma_x^{(f)} \tag{2.c}$$

and

$$\varepsilon_x^{(m)} - \alpha_1^{(m)} T = \frac{\sigma_x^{(m)} - \mu_{12}^{(m)} (\sigma_r^{(m)} + \sigma_\theta^{(m)})}{E_1^{(m)}} \tag{3.a}$$

$$\varepsilon_r^{(m)} - \alpha_1^{(m)} T = \frac{\sigma_r^{(m)} - \mu_{12}^{(m)} (\sigma_\theta^{(m)} + \sigma_x^{(m)})}{E_1^{(m)}} \tag{3.b}$$

$$\varepsilon_\theta^{(m)} - \alpha_1^{(m)} T = \frac{\sigma_\theta^{(m)} - \mu_{12}^{(m)} (\sigma_r^{(m)} + \sigma_x^{(m)})}{E_1^{(m)}} \tag{3.c}$$

where the superscripts f and m denote fiber and matrix, E and μ are Young's modulus and Poisson's ratio, α and T are thermal expansion coefficient and temperature change.

In Fig. 1, the radial displacements $u^{(n)}$ and the axial displacements $w^{(n)}$ for both the fiber and matrix (the superscript n denotes either fiber (when $n = f$) or matrix (when $n = m$)) must satisfy the following equations:

$$\frac{d^2u^{(n)}}{dr^2} + \frac{1}{r}\frac{du^{(n)}}{dr} - \frac{u^{(n)}}{r^2} = 0 \tag{4}$$

$$\frac{d^2w^{(n)}}{dx^2} = 0. \tag{5}$$

The general solution for eqn (4) is:

$$u^{(n)} = \frac{A^{(n)}}{2}r + \frac{B^{(n)}}{r} \tag{6}$$

and the general solution for eqn (5) is:

$$w^{(n)} = C^{(n)}x + D^{(n)} \tag{7}$$

where $A^{(n)}$, $B^{(n)}$, $C^{(n)}$ and $D^{(n)}$ are unknown constants which can be obtained by boundary and interface conditions.

The strains are given by:

$$\varepsilon_x^{(n)} = \frac{dw^{(n)}}{dx} \tag{8.a}$$

$$\varepsilon_f^{(n)} = \frac{du^{(n)}}{dr} \tag{8.b}$$

$$\varepsilon_\theta^{(n)} = \frac{u^{(n)}}{r}. \tag{8.c}$$

Considering eqns (2), (3), (6), (7) and (8) and enforcing the following conditions:

$$u^{(f)} = u^{(m)} \quad \text{and} \quad w^{(f)} = w^{(m)} \quad \text{when } r = r_f \tag{9.a}$$

$$\sigma_r^{(f)} \quad \text{and} \quad \sigma_\theta^{(f)} \neq \infty \quad \text{when } r \to 0 \tag{9.b}$$

$$\sigma_r^{(f)} = \sigma_r^{(m)} \quad \text{when } r = r_f \tag{9.c}$$

$$\sigma_f^{(m)} = 0 \quad \text{when } r = r_m \tag{9.d}$$

$$\int_0^r \sigma_x^{(f)} r dr + \int_{r_f}^{r_m} \sigma_x^{(m)} r dr = 0 \tag{9.e}$$

we can obtain the thermal stress field. For additional details for the solution, the reader is referred to literature (Lanir and Fung, 1972; Steif, 1984; Mikata and Taya, 1985). Figure

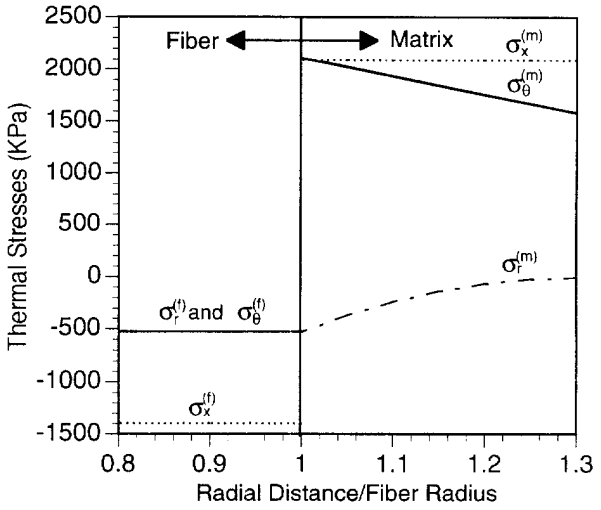

Fig. 2. Thermal stress distribution from the coaxial cylinder model in a T300/5222 composite with a fiber volume fraction $v_f = 0.6$, temperature change $T = -1$°C.

2 shows the thermal residual stresses in a T300/5222 composite with material properties listed in Table 1. The temperature change is set to be -1.0°C without loss of generality.

The Lame's model presents that the mismatch of the thermal expansion coefficients between fiber and matrix results in an axial compressive loading in each fiber when the temperature is decreased. It also shows no shear stresses exist in the fiber-matrix system and the radial stress normal to the fiber-matrix interface is compressive. These results can not explain the reason that debonding occurs in fiber-reinforced composites after curing which may be micrographically observed in experiments. In fact, the axial compressive loading $\sigma_x^{(f)}$ will bend the fiber with initial deflection even though it is significantly lower than the fiber buckling strength and the bending deflection is not linearly dependent on the compressive loading. The matrix acts as an elastic foundation to provide lateral support for the fibers. So the additional thermal residual stresses are deduced associated with the fiber micro-bending.

The compressive response of fiber-reinforced composites under the action of thermal axial compressive loadings in fibers can be investigated by theory of elastic stability (Timoshenko and Gere, 1961). In the analysis of compressive strength of unidirectional composites, two models, based on the shapes of fiber deflection, have been developed. The extensional fiber micro-buckling model (Wass *et al.* 1990) postulated that the buckled deflections of fibers were described by triangular functions and satisfied the Timoshenko beam theory. The displacements of the matrix were determined by classical elasticity. The local fiber micro-buckling model (Hanasaki and Hasegawa, 1974; Yeh and Teply, 1988; Lessard and Chang, 1991) was developed from the principle of minimum potential energy. The deflections of fibers were also postulated to be triangular functions. The strains in matrix were uniform along the transverse direction between two neighboring fibers and the contribution of matrix energy was only made by shear strain. In the present analysis, we consider two cases of initial fiber curvature, extensional fiber misalignments and local fiber

Table 1. The material properties for T300 fiber and 5222 matrix

Longitudinal Modulus	E_1	221.0 GPa	3.8 GPa
Transverse Modulus	E_2	13.8 GPa	
Longitudinal Shear Modulus	G_{12}	9.0 GPa	1.4 GPa
Transverse Shear Modulus	G_{23}	4.8 GPa	
Longitudinal Poisson's Ratio	μ_{12}	0.20	0.35
Transverse Poisson's Ratio	μ_{23}	0.25	
Thermal Expansion Coefficient	α_1	-0.3×10^{-6}/°C	41.0×10^{-6}/°C
Thermal Expansion Coefficient	α_2	3.1×10^{-6}/°C	
Fiber Radius	r_f	3.8×10^{-6} m	

misalignments. Hence, two analytical models, namely extensional micro-bending model and local micro-bending model are developed. In these two models, each fiber is treated as Timoshenko beam and its deflection is assumed to follow a sine law.

4. THEORY FOR THE EXTENSIONAL FIBER MICRO-BENDING (EFB) MODEL

4.1. *Problem formulations*

The configuration of the idealized model is illustrated in Fig. 3. Because the considered fiber-matrix system is infinite and the axial compressive loading $\sigma_x^{(f)}$ applied to each fiber is equal, each fiber is bent in an identical manner, and the interaction between adjacent fibers is null (Lessard and Chang, 1991). We can isolate the analytical model into a fiber and surrounding matrix to perform analysis. Different from the loaded boundary conditions of a compressive loaded fiber-matrix system in the literature (Wass *et al.*, 1990; Hanasaki and Hasegawa, 1974; Yeh and Teply, 1988; Lessard and Chang, 1991), there must be tensile loading $\sigma_x^{(m)}$ applied to the matrix boundaries in a thermal loaded fiber-matrix system because residual stresses in the fiber-matrix system are self-equilibrium. The followings are noted, referred to Fig. 3:

$$c = r_m - r_f \tag{10.a}$$

$$h = 2r_f. \tag{10.b}$$

The initial fiber deflection due to the manufacturing process is assumed to be (Davis, 1975; Hanasaki and Hasegawa, 1974; Yeh and Teply, 1988; Lessard and Chang, 1991):

$$V_i = B_i \sin(\alpha x) \tag{11.a}$$

and an amplitude to half wavelength ratio of initial fiber curvature is defined as:

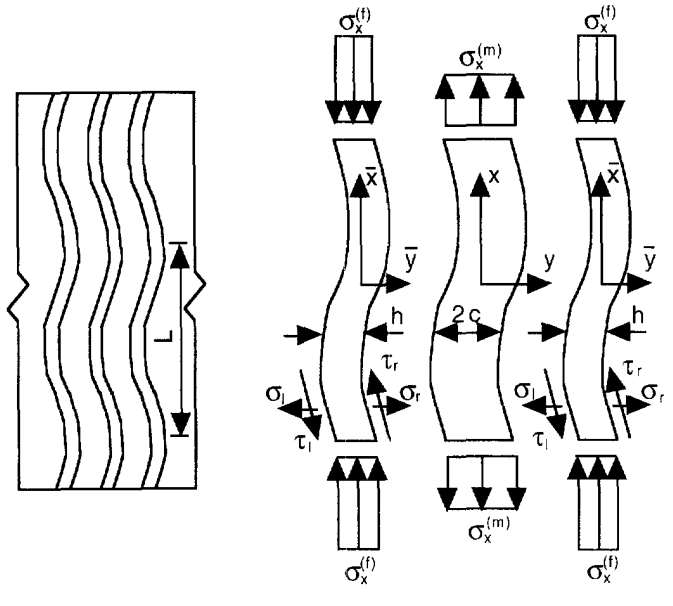

(a) (b)

Fig. 3. The configuration of extensional fiber micro-bending model.

$$e = \frac{2B_i}{L} \tag{11.b}$$

where $\alpha = 2\pi/L$ and L is the bending wavelength.

If we denote V_f and U_f as the lateral deflection and axial displacement of the fibers, and V_m and U_m as the lateral and axial displacements of the matrix, which arise from the fiber micro-bending under the axial compressive loading in each fiber, the continuity conditions of displacements at the fiber-matrix interfaces, base on the assumptions of small plane rotation and middle surface of Timoshenko beam, require:

$$\left[U_f - \frac{h}{2}\frac{\mathrm{d}V_f}{\mathrm{d}x}\right]_{\bar{y}=h/2} = [U_m]_{y=-c} \tag{12.a}$$

$$[V_f]_{\bar{y}=h/2} = [V_m]_{y=-c} \tag{12.b}$$

$$\left[U_f + \frac{h}{2}\frac{\mathrm{d}V_f}{\mathrm{d}x}\right]_{\bar{y}=-h/2} = [U_m]_{y=c} \tag{12.c}$$

$$[V_f]_{\bar{y}=-h/2} = [V_m]_{y=c}. \tag{12.d}$$

Considering each fiber has initial sinusoidal curvature and the displacement continuity conditions in eqns (12.b) and (12.d), we assume that:

$$V_f = B\sin(\alpha x) \tag{13.a}$$

$$V_m = \Phi(y)\sin(\alpha x). \tag{13.b}$$

V_f plus V_i is the total fiber displacement in the lateral direction. Since the lateral displacements V_f and V_m follow a sine law, the axial displacements U_f and U_m must be assumed to follow a cosine law to guarantee displacement continuity at the fiber-matrix surface (see eqns (12.a) and (12.c)), that is:

$$U_f = A\cos(\alpha x) \tag{14.a}$$

$$U_m = \Psi(y)\cos(\alpha x). \tag{14.b}$$

Now the governing equations of a fiber in the bent state are developed. From Fig. 3(b), an infinitesimal beam element of fiber is cut as shown in Fig. 4. The force and moment equilibrium equations for the beam element in the x-y plane are derived as:

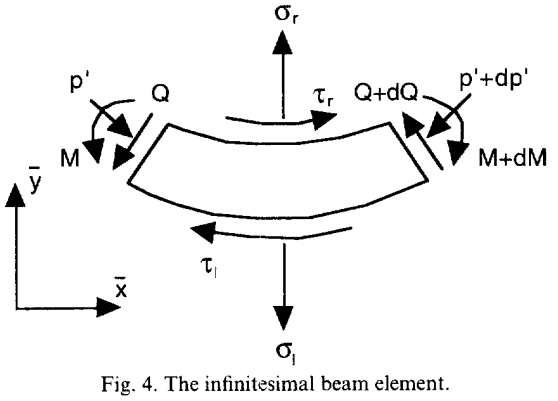

Fig. 4. The infinitesimal beam element.

$$\frac{dp'}{dx} + (\tau_1 - \tau_r) = 0 \tag{15.a}$$

$$\frac{dQ}{dx} + (\sigma_1 - \sigma_r) - \sigma_x^{(f)} h \frac{d^2(V_f + V_i)}{dx^2} = 0 \tag{15.b}$$

$$-\frac{d^2M}{dx^2} - \frac{h}{2}\frac{d(\tau_1 - \tau_2)}{dx} + \frac{dQ}{dx} = 0 \tag{15.c}$$

where p' is the variation of axial force at bending, M is the bending moment in the fiber, σ_r and τ_r, σ_1 and τ_l are the interface stresses at the right and left surfaces of the fiber and Q is the shear loading at the fiber cross-section. In eqn (15.b), the term $p' d^2(V_f + V_i)/dx^2$ has been neglected because it is of second order and the bending is infinitesimal.

From the stress-strain relation and the beam's deflection-moment relation, we obtain:

$$p' = hE_l^{(f)} \frac{dU_f}{dx} \tag{16.a}$$

$$M = -E_l^{(f)} I_f \frac{d^2 V_f}{dx^2} \tag{16.b}$$

where $E_l^{(f)}$ is the longitudinal Young's modulus of the fibers and I_f is the moment of inertia of the fibers that is equal to $h^3/12$. Combining eqns (15) and (16), the governing equations for the bent fibre are developed as follows:

$$E_l^{(f)} I_f \frac{d^4 V_f}{dx^4} + \sigma_x^{(f)} h \frac{d^2(V_f + V_i)}{dx^2} + (\sigma_l - \sigma_r) - \frac{h}{2}\frac{d}{dx}(\tau_l + \tau_r) = 0 \tag{17.a}$$

$$-(\tau_l - \tau_r) + hE_1^{(f)} \frac{d^2 U_f}{dx^2} = 0. \tag{17.b}$$

For the matrix, the equilibrium equations expressed in terms of its displacements in the x-y plane strain state are:

$$2\frac{\partial^2 U_m}{\partial x^2} + (1 - \mu_{12}^{(m)})\frac{\partial^2 U_m}{\partial y^2} + (1 + \mu_{12}^{(m)})\frac{\partial^2 V_m}{\partial x \partial y} = 0 \tag{18.a}$$

$$2\frac{\partial^2 V_m}{\partial y^2} + (1 - \mu_{12}^{(m)})\frac{\partial^2 V_m}{\partial x^2} + (1 + \mu_{12}^{(m)})\frac{\partial^2 U_m}{\partial x \partial y} = 0. \tag{18.b}$$

The overall equilibrium condition of the fiber-matrix system requires:

$$p' + \int_{-c}^{c} \sigma_{xm} dy = 0. \tag{19}$$

Hereafter, the stress and strain components with subscripts f and m denote the residual stresses and strains in fiber and matrix due to fiber micro-bending. Substituting eqns (13.b) and (14.b) into (18) and eliminating Φ, the following fourth order ordinary differential equation for Ψ is obtained:

$$\Psi^{IV} - 2\alpha^2 \Psi'' + \chi^4 \Psi = 0. \tag{20}$$

Similarly, the equation for Φ is:

$$\Phi^{IV} - 2\alpha^2\Phi'' + \alpha^4\Phi = 0. \tag{21}$$

The solutions for eqns (20) and (21), subjected to the conditions in eqns (12), are:

$$\Psi(y) = C_1 \cos h(\alpha y) + C_2 \sin h(\alpha y) + C_3 y \cos h(\alpha y) + C_4 y \sin h(\alpha y) \tag{22}$$

$$\Phi(y) = D_1 \cos h(\alpha y) + D_2 \sin h(\alpha y) + D_3 y \cos h(\alpha y) + D_4 y \sin h(\alpha y). \tag{23}$$

Through eqns (18), C_i and D_i are related by:

$$D_1 = C_2 - \frac{C_3}{\alpha}\left(\frac{3-\mu_{12}^{(m)}}{1+\mu_{12}^{(m)}}\right) \tag{24.a}$$

$$D_2 = C_1 - \frac{C_4}{\alpha}\left(\frac{3-\mu_{12}^{(m)}}{1+\mu_{12}^{(m)}}\right) \tag{24.b}$$

$$D_3 = C_4 \tag{24.c}$$

$$D_4 = D_3. \tag{24.d}$$

Enforcing the restrictions in eqns (12), it is derived that:

$$C_1 = 2m_1 A \tag{25.a}$$

$$C_2 = B(m_2 p + 2m_3) \tag{25.b}$$

$$C_3 = \alpha B(m_4 p + 2m_5) \tag{25.c}$$

$$C_4 = 2\alpha m_6 A. \tag{25.d}$$

The expressions of m_i and p are listed in Appendix A. Based on the linear stress-strain relationships, the additional thermal residual stresses due to fiber micro-bending in the matrix are solved:

$$\sigma_{xm} = \frac{E_1^{(m)}}{(1-\mu_{12}^{(m)2})}\left(\frac{\partial U_m}{\partial x} + \mu_{12}^{(m)}\frac{\partial V_m}{\partial y}\right)$$

$$= \frac{E_1^{(m)}}{(1-\mu_{12}^{(m)2})}(\alpha\Psi + \mu_{12}^{(m)}\Phi')\cos(\alpha x) \tag{26.a}$$

$$\sigma_{ym} = \frac{E_l^{(m)}}{(1-\mu_{12}^{(m)2})}\left(\frac{\partial V_m}{\partial y} + \mu_{12}^{(m)}\frac{\partial U_m}{\partial x}\right)$$

$$= \frac{E_l^{(m)}}{(1-\mu_{12}^{(m)2})}(\Phi' - \mu_{12}^{(m)}\alpha\Phi)\sin(\alpha x) \tag{26.b}$$

$$\tau_{xym} = \frac{E_l^{(m)}}{2(1+\mu_{12}^{(m)})}\left(\frac{\partial U_m}{\partial y} + \frac{\partial V_m}{\partial x}\right)$$

$$= \frac{E_l^{(m)}}{2(1+\mu_{12}^{(m)})}(\Psi' + \alpha\Phi)\cos(\alpha x). \tag{26.c}$$

From the traction continuity conditions at the fiber-matrix interface, the interface stresses are:

$$\sigma_r = [\sigma_{ym}]_{y=-c} \tag{27.a}$$

$$\sigma_l = [\sigma_{ym}]_{y=c} \tag{27.b}$$

$$\tau_r = [\tau_{xym}]_{y=-c} \tag{27.c}$$

$$\tau_l = [\tau_{xym}]_{y=c}. \tag{27.d}$$

Combining eqns (22)–(27), we obtain:

$$\sigma_l = (P_1 A + P_2 B)\sin(\alpha x) \tag{28.a}$$

$$\sigma_r = (\bar{P}_1 A + \bar{P}_2 B)\sin(\alpha x) \tag{28.b}$$

$$\tau_l = (Q_1 A + Q_2 B)\cos(\alpha x) \tag{28.c}$$

$$\tau_r = (\bar{Q}_1 A + \bar{Q}_2 B)\cos(\alpha x) \tag{28.d}$$

where P_i and $\bar{P}_i$, Q_i and $\bar{Q}_i$ are expressed in Appendix A. Substituting eqns (28) into (17) results in:

$$A = 0 \tag{29.a}$$

$$B = \frac{B_i}{\dfrac{\sigma_{cr}}{\sigma_x^{(f)}} - 1} \tag{29.b}$$

where σ_{cr} is the critical compressive loading of the extensional fiber micro-buckling applied to each fiber in unidirectional composites (Wass *et al.*, 1990) and written as:

$$\sigma_{cr} = \frac{1}{\alpha^2 h}(\alpha^4 E_f I_f + 2P_2 + \alpha h Q_2). \tag{30}$$

Hence, the maximum residual stresses at the interface determined by eqns (28) are:

$$\tau_{\max} = Q_2 B \tag{31.a}$$

$$\sigma_{\max} = P_2 B. \tag{31.b}$$

Because A is equal to zero, it is verified that eqn (19) is automatically satisfied. Furthermore, it is deduced that shear and lateral stresses at the right and left surfaces of a fiber have identical values. The stresses in eqns (26) result from the fiber micro-bending induced by the thermal axial compressive stress in each fiber. The total stresses should be the summation of stresses associated with the fiber micro-bending and stresses before fiber micro-bending in the above section (i.e., from the coaxial cylinder model).

4.2. *Results and discussion*

The development of extensional fiber micro-bending model has been completed. It can be seen that thermal residual stresses at fiber-matrix interfaces are functions of the amplitude and wavelength of initial fiber curvature, fiber volume fraction, temperature decrease and material properties of fiber and matrix. To illustrate the results, T300/5222 composites are chosen with fiber and matrix material properties listed in Table 1. The value of e in eqn (11), which is determined by manufacturing quality, should be measured by experiments. For the boron/epoxy system, Davis (1975) experimentally found that the value of e is in the order of 10^{-2}. Yeh and Teply (1988) assumed that e for a kevlar/epoxy system is also in this range in analyzing the compressive response and got a reasonable result. For the graphite/epoxy system, Highsmith *et al.* (1992) experimentally determined that the value of e ranges between 0.01 and 0.1 by an optical microscope method. Hence, the value of e for T300/5222 system is assumed to be from 0.01 to 0.1 in the present analysis.

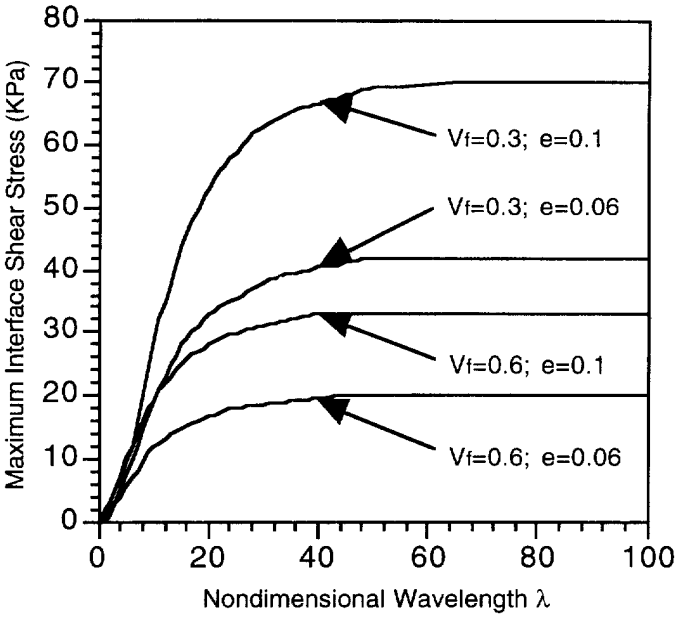

Fig. 5. Variation of maximum residual interface shear stress with nondimensional wavelength λ, temperature decrease $T = -1^{\circ}C$.

The numerical results show that residual lateral stress at the fiber-matrix interface due to fiber micro-bending has a small magnitude compared to the residual interface shear stress. Hence, the discussions are focused on the existence of interface shear stress and we also conclude that debonding at interface associated with temperature decrease arises from thermal residual shear stress.

In Fig. 5, variation of maximum interface shear stress with nondimensional wavelength λ ($\lambda = L/h$) is plotted for T300/5222 composites with various fiber volume fractions v_f and amplitude to half wavelength ratios e. These plots show a continuous dependence of τ_{max} on wavelength λ for given values of e. In a small range of nondimensional wavelength (typically $\lambda < 30$ in Fig. 5), the maximum shear stress changes sharply with λ. However, τ_{max} arrives at a corresponding limited value when the nondimensional wavelength λ is large enough (when $\lambda > 60$ in Fig. 5). This implies that the interface shear stress has an upper bound value for a given value of e when the fibers have initial imperfections with long wavelengths. In the following, we discuss the upper bound interface shear stress.

The admissible residual interface shear stress, which is defined by the limited value in Fig. 5, vs fiber volume fraction v_f is shown in Fig. 6. These plots demonstrate a lower value of τ_{max} for a composite with higher fiber volume fraction. This is because a fiber-matrix system with higher v_f is better able to resist bending (i.e., higher value of buckling strength σ_{cr} in eqn (30)) and the axial compressive loading $\sigma_x^{(f)}$ in the fiber is smaller, thus making the term $\sigma_{cr}\sigma_x^{(f)}$ in eqn (29.b) much smaller. In aeronautical structures, the fiber volume fraction is 0.6 or more for most fiber-reinforced composites based on the requirement of strength and stiffness.

In Fig. 7, variation of the upper bound τ_{max} with temperature decrease is presented. In the conventional models, thermal stresses in fiber-reinforced composites linearly depend on the magnitude of temperature change. It can be seen from eqns (29) and (31) that thermal residual stresses are not a linear function of temperature decrease T in the present model because of the existence of initial fiber curvature. However, numerical results show that the variation of thermal residual stresses with temperature decrease is nearly linear when the magnitude of temperature decrease is in the order of 10^2. This can be explained by the reason that the value of $\sigma_{cr}/\sigma_x^{(f)}$ in eqn (29.b) is much greater than unit for small temperature decrease in this range.

Figure 8 shows effects of initial fiber deflection on the upper bound magnitudes of maximum residual interface shear stress for various v_f. The magnitude of τ_{max} linearly

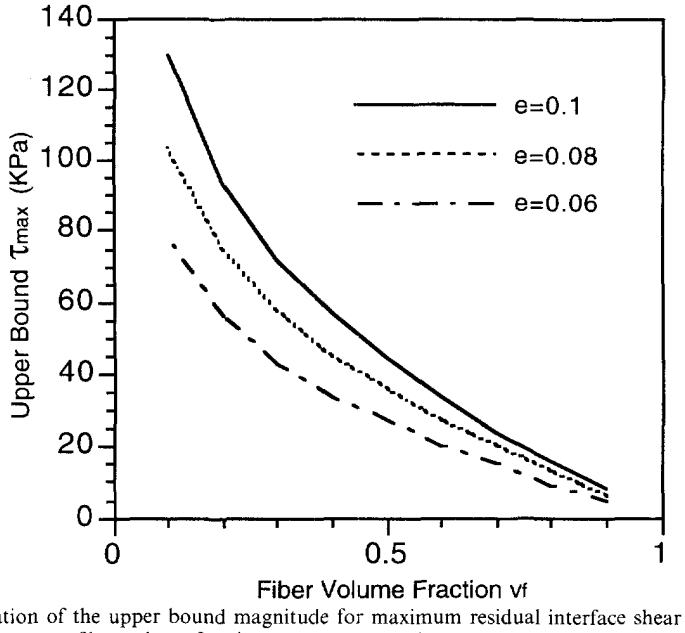

Fig. 6. Relation of the upper bound magnitude for maximum residual interface shear stress and fiber volume fraction v_f, temperature decrease $T = -1°C$.

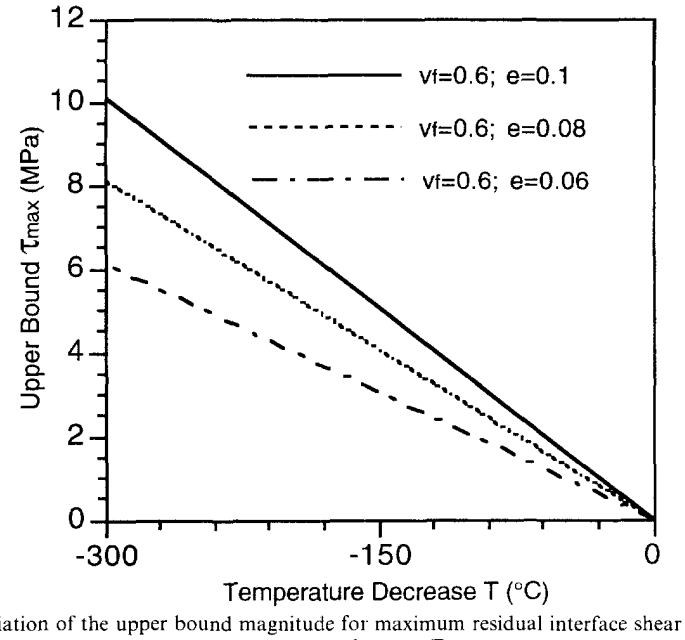

Fig. 7. Variation of the upper bound magnitude for maximum residual interface shear stress with temperature decrease T.

depends on the amplitude to half wavelength ratio e. From eqns (29.b) and (30), we find that the magnitude of maximum interface shear stress is proportional to the amplitude of initial fiber curvature. Therefore, it is important to improve manufacturing quality to reduce the initial deflection of fibers. Because the fiber volume fraction is determined by the requirement of strength and stiffness of composite materials and temperature range is determined by the requirement of curing cycle, improvement of manufacturing quality is the only way to reduce thermal residual stresses in fiber-reinforced composites.

5. THEORY FOR THE LOCAL FIBER MICRO-BENDING (LFB) MODEL

5.1. *Problem formulations*

The configuration of the analytical model is shown in Fig. 9. For the same reason mentioned in the previous section, the model is also isolated into a fiber and surrounding

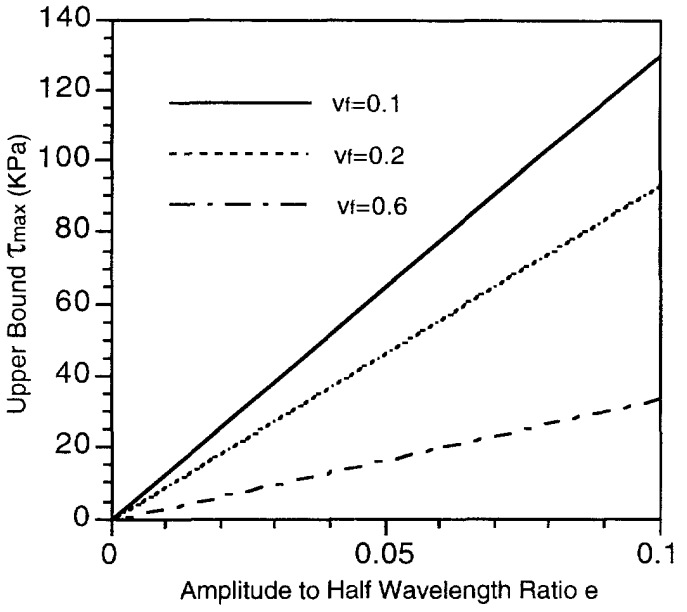

Fig. 8. Effect of the amplitude to half wavelength ratio e on the upper bound magnitude for maximum residual interface shear stress, temperature decrease $T = -1^{\circ}C$.

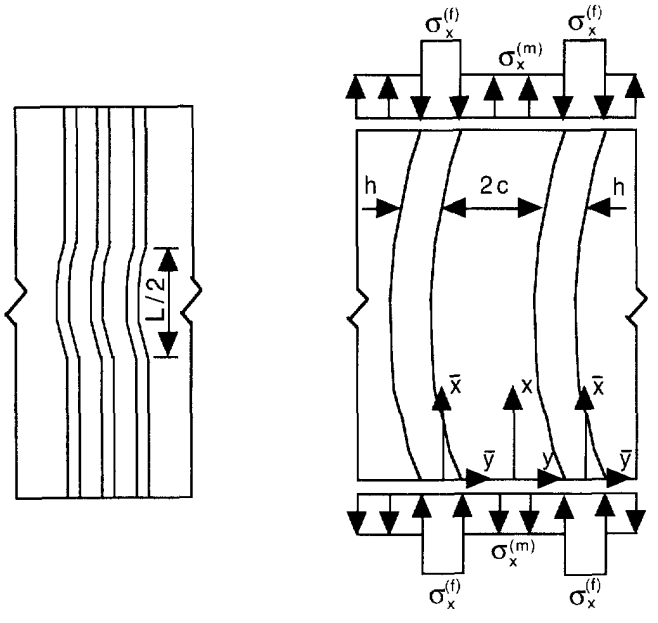

(a) (b)

Fig. 9. The configuration of local fiber micro-bending model.

matrix. The displacements for each fiber and the matrix due to fiber micro-bending are defined to be the same as in eqns (13) and (14). Thus the matrix strains are derived by:

$$\varepsilon_{xm} = -\alpha\Psi(y)\sin(\alpha x) \tag{32.a}$$

$$\varepsilon_{ym} = \Phi'(y)\sin(\alpha x) \tag{32.b}$$

$$\gamma_{xym} = [\Psi'(y)+\alpha\Phi(y)]\cos(\alpha x). \tag{32.c}$$

The total potential energy of the system can be divided into five parts:

$$\Pi = \Pi_f + \Pi_{ft} + \Pi_m + \Pi_{mt} + W \tag{33}$$

where Π_f and Π_m are strain energies in the fiber and the matrix due to fiber micro-bending, Π_{ft} and Π_{mt} are work in the fiber and the matrix done by thermal residual stresses from the coaxial cylinder model (i.e., before fiber micro-bending) on the corresponding deformations due to fiber micro-bending, and W is work done by the boundary applied residual loadings. They can be expressed, respectively, as:

$$\Pi_f = \frac{E_l^{(f)} h}{2} \int_0^{L/2} \left(\frac{\mathrm{d}U_f}{\mathrm{d}x}\right)^2 \mathrm{d}x + \frac{1}{2} E_l^{(f)} I_f \int_0^{L/2} \left(\frac{\mathrm{d}^2 V_f}{\mathrm{d}x^2}\right)^2 \mathrm{d}x \tag{34.a}$$

$$\Pi_{ft} = \int_v \sigma_x^{(f)} \varepsilon_{xf} \mathrm{d}v \tag{34.b}$$

$$\Pi_m = \frac{1}{2} \int_v \left[\frac{E_l^{(m)}}{(1-\mu_{12}^{(m)2})} (\varepsilon_{xm}^2 + \varepsilon_{ym}^2 + 2\mu_{12}^{(m)} \varepsilon_{xm} \varepsilon_{ym}) + \frac{E_l^{(m)}}{2(1+\mu_{12}^{(m)})} \gamma_{xym}^2 \right] \mathrm{d}v \tag{34.c}$$

$$\Pi_{mt} = \int_v \overline{\sigma_r^{(m)}} \varepsilon_{ym} \mathrm{d}v + \int_v \sigma_x^{(m)} \varepsilon_{xm} \mathrm{d}v \tag{34.d}$$

$$W = \sigma_x^{(m)} \int_{-c}^{c} 2\Psi \mathrm{d}y - \sigma_x^{(f)} h \left\langle 2A + \frac{1}{2} \int_0^{L/2} \left\{ \left[\frac{\mathrm{d}^2 (V_f + V_i)}{\mathrm{d}x^2} \right]^2 \left(\frac{\mathrm{d}V_i}{\mathrm{d}x} \right)^2 \right\} \mathrm{d}x \right\rangle. \tag{34.e}$$

In eqn (34.d), the radial stress $\sigma_r^{(m)}$ form the coaxial cylinder model is approximately replaced by its average value $\bar{\sigma}_f^{(m)}$ along the y axis for the reason of simplicity. This approximation is acceptable because the magnitude of $\sigma_r^{(m)}$ is much smaller than those of $\sigma_x^{(m)}$ and $\sigma_\theta^{(m)}$ (see Fig. 2).

Combining the related equations and integrating with respect to x from zero to $L/2$, the following equation is given:

$$\Pi = \frac{L}{8} \{ \alpha^2 E_l^{(f)} h A^2 + \alpha^4 E_l^{(f)} I_f B^2 + \int_{-c}^{c} \left[\frac{E_l^{(m)}}{(1-\mu_{12}^{(m)2})} (\alpha^2 \Psi^2 - \alpha \mu_{12}^{(m)} \Psi \Phi') + \frac{E_l^{(m)}}{(1-\mu_{12}^{(m)2})} \left(\Phi^2 - \alpha \mu_{12}^{(m)} \Psi \Phi' + \frac{E_l^{(m)}}{2(1+\mu_{12}^{(m)})} \Psi' + \alpha \Phi \right)^2 + \frac{4}{\alpha} \overline{\sigma_r^{(m)}} \Phi' \right] \mathrm{d}y + 2\alpha^2 \sigma_x^{(f)} h (B^2 + 2BB_i) \}. \tag{35}$$

Using standard procedure of calculus of variation, the minimization of total potential energy Π in eqn (35) must satisfy the following Euler–Poisson's equation:

$$\frac{\mathrm{d}}{\mathrm{d}y} \left(\frac{\partial \Pi}{\partial \Psi'} \right) - \frac{\partial \Pi}{\partial \Psi} = 0 \tag{36}$$

$$\frac{\mathrm{d}}{\mathrm{d}y} \left(\frac{\partial \Pi}{\partial \Phi'} \right) - \frac{\partial \Pi}{\partial \Phi} = 0. \tag{37}$$

Thus, the following equations are developed:

$$2\alpha^2 \Psi - (1-\mu_{12}^{(m)}) \Psi'' - \alpha (1+\mu_{12}^{(m)}) \Phi' = 0 \tag{38}$$

$$2\Phi'' - \alpha^2 (1-\mu_{12}^{(m)}) \Phi - \alpha (1+\mu_{12}) \Psi' = 0. \tag{39}$$

It is interesting that the governing equations for the two functions Ψ and Φ, obtained by minimizing the potential energy have the same forms as by theory of classical elasticity. Therefore, the general solutions of eqns (38) and (39) are obtained in a fashion similar to the previous section, and then all the constants in the general solutions of Ψ and Φ in both EFB model and LFB model are represented by the two constants A and B from the displacement continuity conditions at the fiber-matrix interface. However, the two constants A and B in EFB model are determined by the traction continuity conditions and the equilibrium equations of Timoshenko beam, while the two constants A and B in LFB model are determined by minimizing the potential energy of the system.

Substituting functions Ψ and Φ into eqn (35), the summation of potential energy of the system is in terms of two variables A and B. Minimizing the potential energy with respect to these variables

$$\frac{\partial \Pi}{\partial A} = 0 \tag{40}$$

$$\frac{\partial \Pi}{\partial B} = 0 \tag{41}$$

results in the solutions of A and B:

$$A = 0 \tag{42.a}$$

$$B = \frac{B_i}{\dfrac{\sigma_{cr}}{\sigma_x^{(f)}} - 1} \tag{42.b}$$

where σ_{cr} is the critical compressive loading of fiber local micro-buckling applied to each fiber in unidirectional composites (Yeh and Teply, 1988; Lessard and Chang, 1991) and written as:

$$\sigma_{cr} = \frac{1}{\alpha^2 h}(\alpha^4 E_f I_f + H_1 J_1 + H_2 J_2 + H_3 J_3 + H_4 J_4 + H_5 J_5) \tag{43}$$

and the notations H_i and J_i are listed in Appendix B. The maximum thermal residual stresses at the fiber-matrix interface have the same modes as in eqns (31):

$$\tau_{\max} = Q_2 B \tag{44.a}$$

$$\sigma_{\max} = P_2 B. \tag{44.b}$$

5.2. *Results and discussions*

The analytical model of thermal residual stresses for fiber local micro-bending has been developed. Results are computed for T300/5222 composites. Similar to the results of EFB model, the maximum thermal residual stresses have limited values when the wavelength L is large enough. Also, we discuss this upper bound magnitude of maximum interface shear stress in the present numerical example.

Numerical results show that P_1, P_2 and Q_1 are all much smaller than Q_2, thus, fiber, micro-bending results in additional shear stress that is much larger than additional lateral stress at the fiber-matrix interface. Hence, it is concluded that the supporting effect of matrix to fiber bending is dominated by matrix shear deformation. So it is reasonable that the authors (Hanasaki and Hasegawa, 1974; Yeh and Teply, 1988; Lessard and Chang, 1991) only considered the contribution of matrix shear strain energy to the total potential energy of the fiber matrix-system.

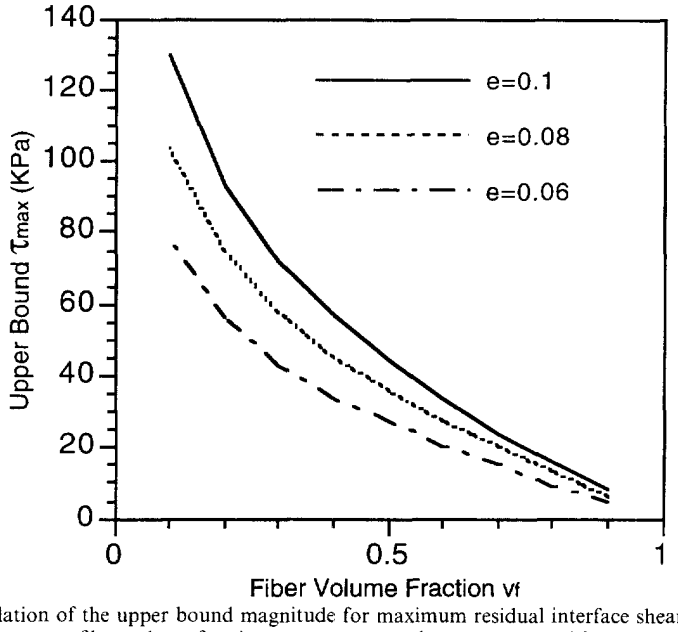

Fig. 10. Relation of the upper bound magnitude for maximum residual interface shear stress and fiber volume fraction v_f, temperature decrease $T = -1°C$.

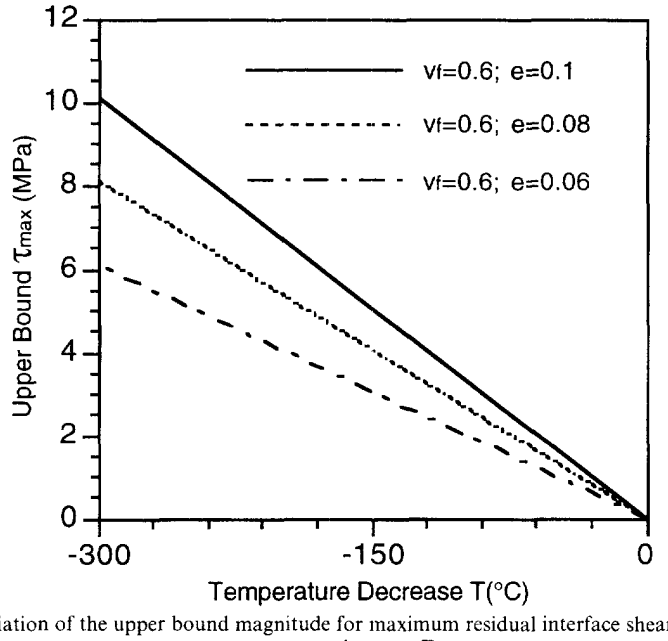

Fig. 11. Variation of the upper bound magnitude for maximum residual interface shear stress with temperature decrease T.

The relation of the upper bound magnitude of maximum residual shear stress at the fiber-matrix interface and fiber volume fraction for LFB model is shown in Fig. 10. The variation of the upper bound τ_{max} with temperature decrease T is shown in Fig. 11. The effect of e on the upper bound magnitude of τ_{max} is presented in Fig. 12. It is found that the results for the upper bound values of maximum interface shear stress from EFB model and LFB model are very close. Comparing the formulations of EFB model and LFB model, the difference that we can find is between the critical compressive loading of extensional fiber micro-buckling in eqn (30) and that of local fiber micro-buckling in eqn (43). The critical compressive loadings of these two fiber micro-buckling modes have limited values when the wavelength is large enough (Wass *et al.*, 1990), and these two buckling strengths are very close to each other. This is the reason why the upper bound magnitudes of maximum interface shear stresses in the extensional fiber micro-bending mode and the local

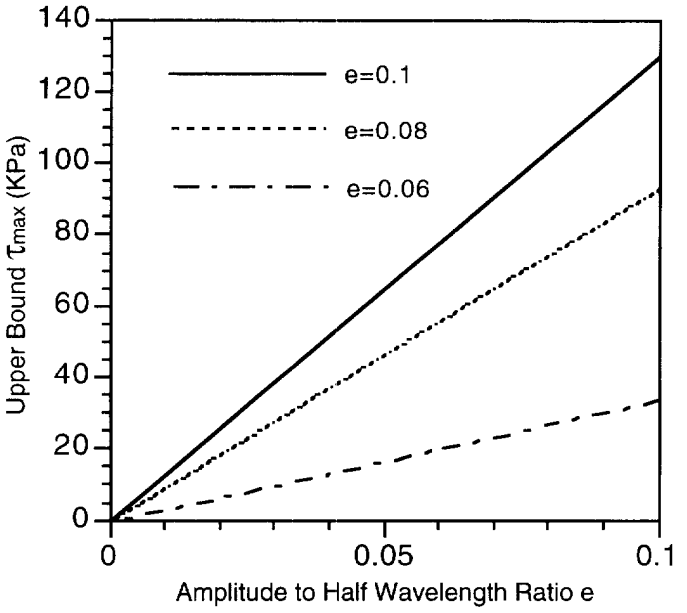

Fig. 12. Effect of the amplitude to half wavelength ratio e on the upper bound magnitude for maximum residual interface shear stress, temperature decrease $T = -1\,^{\circ}C$.

fiber micro-bending mode are almost identical, if the extensional initial fiber curvature and local initial fiber curvature have the same ratio of amplitude to wavelength.

6. CONCLUSIONS

An analytical model has been set up for predicting thermal residual stresses at the fiber-matrix interface in fiber-reinforced composites. Both solutions for extensional fiber misalignment model and local fiber misalignment model are completed respectively. It is important to combine two models to form a complete solution because both the fiber imperfection modes may occur in fiber-reinforced composites. The results are very useful to explain some microscopic phenomena of fiber-reinforced composites. The following conclusions can be made:

1. The thermal residual shear stress at the fiber-matrix interface results from temperature decrease during curing process and initial fiber imperfections which are unavoidable in fiber-reinforced composites through manufacturing process.
2. The magnitude of thermal residual interface shear stress depends on fiber volume fraction, material properties and the wavelength and amplitude of fiber initial curvature. The greater the fiber volume fraction, the smaller the shear stress is. The interface shear stress linearly depends on the amplitude to wavelength ratio of initial fiber curvature, thus the manufacturing technique is a key factor to reduce its magnitude.
3. There is an approximately linear relationship between thermal residual stresses and temperature drop when the magnitude of the drop is in the order of 10^2.
4. The supporting action of matrix to fiber-bending is dominated by matrix shear deformation. So the energy due to matrix normal deformation can be omitted for predicting the fiber buckling strength by energy principle.
5. There exist upper bound magnitudes of maximum residual shear stress at the fiber-matrix interface for both extensional fiber micro-bending mode and local fiber micro-bending mode with long wavelengths. These two upper bound magnitudes are very close when the extensional initial fiber curvature and local initial fiber curvature have the same amplitude to wavelength ratio. Therefore, thermal residual stresses in a unidirectional fiber-reinforced composite system can be computed from either of the two fiber misalignment models if the amplitude to half wavelength ratio e of the system is known.

Acknowledgments—The authors wish to acknowledge the two anonymous reviewers' comments that were very helpful in revisions.

REFERENCES

Banbaji, J. (1988) On a more generalized theory of pull-out test from an elastic matrix: part II—application to a polypropylene-cement system. *Composites Science and Technology* **32**, 195–207.
Brewer, J. C. and Lagace, P. A. (1988) Quadratic stress criterion for initiation of delamination. *Journal of Composite Materials* **22**, 1141–1155.
Davis, J. G. (1975) Compressive strength of fiber-reinforced composite materials. Composite Reliability, ASTM STP **580**, pp. 364–377.
Hahn, H. T. and Williams, J. G. (1984) Compression failure mechanisms in unidirectional composites. NASA TM 85843.
Hahn, H. T., Sohi, M. and Moon, S. (1986) Composite failure mechanism of composite materials. NASA Report 3989.
Hanasaki S. and Hasegawa, Y. (1974) Compressive strength of unidirectional fibrous composites. *Journal of Composite Materials* **8**, 306–309.
Herrmann, L. R., Mason, W. E. and Chan, S. T. K. (1967) Response of reinforcing wires to compressive states of stress. *Journal of Composite Materials* **1**, 212–226.
Highsmith, A. L., Davis, J. J. and Helms, L. E. (1992) The influence of fiber waviness on the compressive behaviour of unidirectional continuous fiber composites. Composite Materials: Testing and Design. ASTM STP **1120**, pp. 20–36.
Hojjati, M. (1994) Curing of thick thermosetting composites: experiment, simulation and scaling. Ph.D. dissertation, Concordia University, Montreal, Canada.
Iesan, D. (1980) Thermal stresses in composite cylinders. *Journal of Thermal Stress* **3**, 495–508.
Jayaraman, K. and Reifsnider, K. L. (1993) The interphase in unidirectional fiber-reinforced epoxies: effect on residual thermal stresses. *Composites Science and Technology* **47**, 119–129.
Kalantar, J. and Drzal, L. T. (1990) The boundary mechanism of aramid fibers to epoxy matrices: part II—an experimental investigation. *Journal of Material Science* **25**, 4194–4202.
Lanir, J. and Fung, Y. C. B. (1972) Fiber composite columns under compression. *Journal of Composite Material* **6**, 387–401.
Lessard, B. L. and Chang, F. K. (1991) Effect of load distribution on the fiber buckling strength of unidirectional composites. *Journal of Composite Materials* **25**, 65–87.
Mikata, Y. and Taya, M. (1985) Stress field in a coated continuous fiber composite subject to thermo-mechanical loadings. *Journal of Composite Materials* **19**, 554–571.
Pagano, N. J. and Tandon, G. P. (1988) Elastic response of multidirectional coated-fiber composites. *Composites Science and Technology* **31**, 272–293.
Powell, K. L., Smith, P. A. and Yeomans, J. A. (1993) Aspects of residual thermal stresses in continuous-fiber-reinforced ceramic matrix composites. *Composites Science and Technology* **47**, 359–367.
Slaughter, W. S. and Fleck, N. A. (1994) Microbuckling of fiber composites with random initial fiber waviness. *Journal of the Mechanics and Physics of Solids* **42**, 1743–1766.
Steif, P. S. (1984) Stiffness reduction due to fiber breakage. *Journal of Composites Materials* **17**, 153–172.
Strong, A. B. (1989) *Fundamentals of Composite Manufacturing: Materials, Methods, and Applications*. Society of Manufacturing Engineer, Michigan.
Timoshenko, S. P. and Gere, J. M. (1961) *Theory of Elastic Stability*, 2nd edition. McGraw-Hill, New York.
Wass, A. M., Babcock, C. D. and Knauss, W. G. (1990) A mechanical model for elastic fiber microbuckling. *Journal of Applied Mechanics* **57**, 138–149.
Yeh, J. R. and Teply, J. L. (1988) Compressive response of kevlar/epoxy composites. *Journal of Composite Materials* **22**, 245–257.

APPENDIX A

The expressions used in the text are:

$$m_1 = \frac{-\cos h(\alpha c) + \frac{2K}{pq}\sin h(\alpha c)}{\Delta^*} \tag{A.1}$$

$$m_2 = \frac{-\sin h(\alpha c) + \frac{2K}{pq}\cos h(\alpha c)}{\Delta^{**}} \tag{A.2}$$

$$m_3 = \frac{\cos h(\alpha c)}{\Delta^{**}} \tag{A.3}$$

$$m_4 = \frac{2\cos h(\alpha c)}{pq\Delta^{**}} \tag{A.4}$$

$$m_5 = -\frac{2\sin h(\alpha c)}{pq\Delta^{**}} \tag{A.5}$$

$$m_6 = \frac{2\sin h(\alpha c)}{pq\Delta^*} \tag{A.6}$$

where:

$$p = \frac{2\pi h}{L} \tag{A.7}$$

$$q = \frac{2c}{h} \tag{A.8}$$

$$K = \frac{3-\mu_{12}^{(m)}}{1+\mu_{12}^{(m)}} \tag{A.9}$$

$$\Delta^* = \frac{2K}{pq}\sin h(2\alpha c) - 2 \tag{A.10}$$

$$\Delta^{**} = \frac{2K}{pq}\sin h(2\alpha c) + 2 \tag{A.11}$$

and

$$P_1 = \{2m_1 \cos h(\alpha c)(1-\mu_{12}^{(m)}) + m_6[2\cos h(\alpha c)(1-K) + pq\sin h(\alpha c)(1-\mu_{12}^{(m)})]\}\frac{E_1^{(m)}\alpha}{(1-\mu_{12}^{(m)^2})} \tag{A.12}$$

$$P_2 = \{2m_2 p\sin h(\alpha c)(1-\mu_{12}^{(m)}) + 2m_3\sin h(\alpha c)(1-\mu_{12}^{(m)}) + m_4[p\sin h(\alpha c)(1-K) + \frac{1}{2}p^2 q\cos h(\alpha c)(1-\mu_{12}^{(m)})] - m_5[2\sin h(\alpha c)(1-K) + pq\cos h(1-\mu_{12}^{(m)})]\}\frac{E_1^{(m)}\alpha}{(1-\mu_{12}^{(m)^2})} \tag{A.13}$$

$$\overline{P_1} = P_1 \tag{A.14}$$

$$\overline{P_2} = -P_2 \tag{A.15}$$

$$Q_1 = \{2m_1\sin h(\alpha c) + m_6[\sin h(\alpha c)(1-K) + pq\cos h(\alpha c)]\}\frac{E_1^{(m)}\alpha}{(1+\mu_{12}^{(m)})} \tag{A.16}$$

$$Q_2 = \{2m_2 p\cos h(\alpha c) + 4m_3\cos h(\alpha c) + m_4 p[\cos h(\alpha c)(1-K) + pq\sin h(\alpha c)] + 2m_5[\cos h(\alpha c)(1-K) + pq\sin h(\alpha c)]\}\frac{E_1^{(m)}\alpha}{2(1+\mu_{12}^{(m)})} \tag{A.17}$$

$$\overline{Q_1} = -Q_1 \tag{A.18}$$

$$\overline{Q_2} = Q_2. \tag{A.19}$$

APPENDIX B

$$H_1 = \frac{E_1^{(m)}}{(1+\mu_{12}^{(m)})}[\alpha\overline{c_2} + \overline{c_3}) + \alpha\overline{d_1}]^2 \tag{B.1}$$

$$H_2 = \frac{2E_1^{(m)}}{(1-\mu_{12}^{(m)^2})}[\alpha^2\overline{c_2^2} - 2\alpha\mu_{12}^{(m)}(\alpha\overline{d_1} + \overline{d_4})\overline{c_2} + (\alpha\overline{d_1} + \overline{d_4})^2] \tag{B.2}$$

$$H_3 = \frac{4E_1^{(m)}}{(1-\mu_{12}^{(m)^2})}[\alpha^2\overline{c_2 c_3} - \alpha\mu_{12}^{(m)}(\alpha\overline{c_2 d_4} + \alpha\overline{c_3 d_1} + \overline{c_3 d_4}) + \alpha\overline{d_4}(\alpha\overline{d_1} + \overline{d_4})] + \frac{2E_1^{(m)}\alpha}{(1+\mu_{12}^{(m)})}[\overline{c_3}(\alpha\overline{c_2} + \overline{c_3}) + \overline{d_4}(\alpha\overline{c_2} + \overline{c_3}) + \alpha\overline{d_1}(\overline{c_3} + \overline{d_4})] \tag{B.3}$$

$$H_4 = \frac{E_1^{(m}\alpha^2}{(1+\mu_{12}^{(m)})}(\overline{c_3} + \overline{d_4})^2 \tag{B.4}$$

$$H_5 = \frac{2E_1^{(m)}\alpha^2}{(1-\mu_{12}^{(m)^2})}(\overline{c_3^2} - 2\mu_m \overline{c_3 d_4} + \overline{d_4^2}) \tag{B.5}$$

where:

$$\overline{c_1} = 2m_1 \tag{B.6}$$

$$\overline{c_2} = pm_2 + 2m_3 \tag{B.7}$$

$$\overline{c_3} = \alpha(pm_4 + 2m_5) \tag{B.8}$$

$$\overline{c_4} = 2\alpha m_6 \tag{B.9}$$

$$\overline{d_1} = (pm_2 + 2m_3) - K(pm_4 + 2m_5) \tag{B.10}$$

$$\overline{d_2} = 2m_1 - 2Km_6 \tag{B.11}$$

$$\overline{d_3} = 2\alpha m_6 \tag{B.12}$$

$$\overline{d_4} = \alpha(pm_4 + 2m_5) \tag{B.13}$$

and

$$J_1 = \frac{1}{2}c + \frac{1}{4\alpha}\sin h(2\alpha c) \tag{B.14}$$

$$J_2 = -\frac{1}{2}c + \frac{1}{4\alpha}\sin h(2\alpha c) \tag{B.15}$$

$$J_3 = \frac{1}{4\alpha}c\cos h(2\alpha c) - \frac{1}{8\alpha^2}\sin h(2\alpha c) \tag{B.16}$$

$$J_4 = \frac{1}{4\alpha}c^2\sin h(2\alpha c) - \frac{1}{4\alpha^2}c\cos h(2\alpha c) + \frac{1}{8\alpha^3}\sin h(2\alpha c) - \frac{1}{6}c^3 \tag{B.17}$$

$$J_5 = \frac{1}{4\alpha}c^2\sin h(2\alpha c) - \frac{1}{4\alpha^2}c\cos h(2\alpha c) + \frac{1}{8\alpha^3}\sin h(2\alpha c) + \frac{1}{6}c^3. \tag{B.18}$$